Adsorption (2008) 14: 1–9
DOI 10.1007/s10450-007-9013-9

Characterization of two single-wall carbon nanotubes samples by Ar and Kr adsorption isotherms

V. Goudon · J.C. Lasjaunias

Received: 18 April 2006 / Revised: 14 December 2006 / Accepted: 6 July 2007 / Published online: 21 September 2007

Abstract We investigated by Ar and Kr adsorption isotherm techniques for two kinds of carbon single-wall nanotube bundles prepared by different synthesis methods. Despite the difference in the adsorption capacity in the two samples, the adsorption mechanisms are similar, which indicates that the same adsorption sites are involved for Ar and Kr. We have already measured a similar difference in the adsorbed amount in these samples studied by a low-temperature heat-capacity technique, i.e., for the case of ^{4}He as adsorbate. These results cannot be easily explained by only taking into account the topology of the bundles if all tubes are closed-ended. A larger spread of effective surface areas among different sources of samples is reported in the literature data.

Keywords Carbon nanotubes · Adsorption isotherms · Adsorption sites

Abbreviations

Ar	Argon
Kr	Krypton
^{4}He	Helium isotope 4
Xe	Xenon
H_2	Hydrogen
CH_4	Methane
Ne	Neon
SWNT	Single-wall nanotubes
IC	Interstitial channel
AD	Arc discharge
LV	Laser vaporization

V. Goudon (✉) · J.C. Lasjaunias
Centre de Recherches sur les Très Basses Températures, CNRS, associé à l'UJF, BP 166, 38042 Grenoble cedex 9, France
e-mail: valerie.goudon@grenoble.cnrs.fr

S_{eff}	Effective surface area, in $m^2 \cdot g^{-1}$
τ	Time constant, in s
P_0	Saturated vapor pressure, in Torr
V_{ads}	Adsorbed volume STP, in $cm^3 \cdot g^{-1}$ or $cm^3 \cdot g^{-1} \cdot$Torr
σ	Area occupied by one atom of the adsorbate, in $Å^2$

1 Introduction

The adsorption of gases on closed-ended carbon nanotubes has been the subject of intensive experimental and theoretical investigations during the last five years (see, for instance, Bienfait et al. 2004; Gatica et al. 2001). Rare gases like Ar, Kr, Xe and also ^{4}He, H_2 and CH_4 have been studied mainly by adsorption isotherms, but also by neutron diffraction or heat capacity techniques.

To a first approximation, one can describe the arrangement of identical single-wall nanotubes (SWNT) as a regular hexagonal lattice (Fig. 1). Three adsorption sites are available: 1D interstitial channels (IC's) (only for small molecules like Ne, H_2 or He) (Stan et al. 2000), external grooves at the junction of two individual tubes and then the outer graphene surfaces. The controversy about the possibility for larger molecules like Ar, Kr, CH_4, etc… to adsorb into the IC's was partially resolved by the hypothesis of heterogeneous bundles, due to a possible distribution of tube diameters, with a few defective, larger IC's (Shi and Johnson 2003). From the adsorption isotherm technique alone, it is very difficult to distinguish between the IC's and external grooves sites.

Within this context, we present a comparative study of adsorption of Ar and Kr rare gases in two different kinds of single-wall carbon nanotube bundles, that we have previously studied by a low-temperature heat capacity technique,

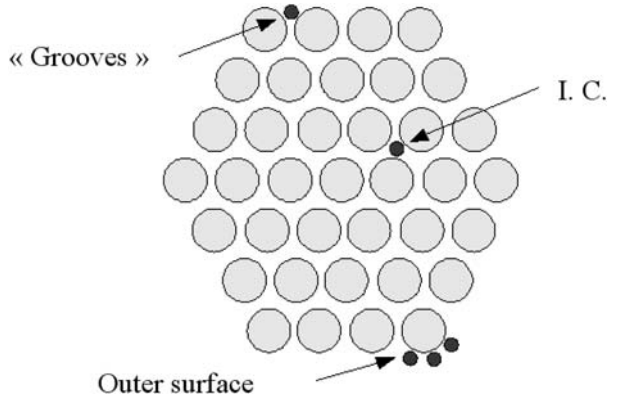

Fig. 1 Schematic representation of an homogeneous bundle of SWNT with the 3 adsorption sites

successively in their out-gassed state and thereafter with ^{4}He adsorbed (Lasjaunias et al. 2002, 2003a, 2003b). These two species, one synthesized by the arc-discharge (AD) method and the other by laser vaporization (LV), differ mainly by the mean number of tubes per bundle, the individual tube diameter being similar (1.4 nm), and hence by different ratios of 1D and 2D sites (Lasjaunias et al. 2003a, 2003b). Two main conclusions were obtained from this previous study: (i) either a 1D to 2D regime for the low temperature heat capacity was measured depending on the amount of adsorbate, in agreement with a crossover from 1D to 2D sites on increasing this density. Such a crossover was later confirmed by neutron diffraction experiments (Pearce et al. 2005), (ii) one species (LV) had an adsorption capacity which is roughly larger than the other by a factor of two, per unit mass of sample.

These properties are presently confirmed by the adsorption studies of the rare gases Ar and Kr, despite the different atom sizes compared to ^{4}He.

In the case of Ar and Kr, we obtain an excellent agreement between the effective surface areas S_{eff}, estimated from the completion of the first monolayer, for each gas. We also recover for each gas a similar ratio of S_{eff} between the two NT species, which confirm our earlier findings for ^{4}He by heat capacity measurements.

2 Experiments

We have measured two kinds of SWNT samples, synthesized by the same procedures as that used for our thermodynamic experiments (Lasjaunias et al. 2002, 2003a, 2003b). X-ray, neutron diffraction, and Raman experiments were systematically used for the characterization of both kinds of samples (Rols et al. 1999, 2000; Almairac and Sauvajol 2002). The first sample was synthesized in Montpellier by the arc-discharge method (Lasjaunias et al. 2003a), with Ni (0.5 at.%) and Y (0.5 at.%) catalysts, in total 1 at.%, with no Co. The bundles are estimated to consist of less than 20–30 closed-ended tubes, 1.4 nm in diameter with a standard deviation of 0.2 nm. The final sample is in the form of a pressed pellet (pressurization at 10 kBar) of 15.2 mg weight, 5 mm diameter. This sample is referred as to "AD-pellet".

The second sample (from Rice University) was synthesized by laser vaporization at 1100 °C with Ni and Co catalysts (up to 2 at.%, as residual concentration in final samples); after acid purification and filtration process, which removes in particular amorphous C and graphitic impurities, the final form is a bucky-paper sheet of several cm^2 area. The bundles are estimated to contain 30 to 50 tubes of a similar diameter (1.4 nm) as in AD samples, from X-ray and neutron diffraction measurements performed on our previous sample (Lasjaunias et al. 2002, 2003a). Acid purification can result in a possible small fraction of open-ended tubes. We used around 7 bands cut from the initial sheet, of total mass 22 mg and estimated area of 9 cm^2. This sample is referred in the following, to as the "bucky-paper" sample.

From the diffraction spectra obtained on the samples used in the thermodynamic experiments, the purity of both samples is essentially similar, with even less carbon nanoshells, amorphous carbon and graphitic impurities in the bucky-paper sample. However, this latter sample contains residual nanoparticles (about 30 nm size) of Co catalyst, in an amount of about 1 at.%, as also determined from the heat capacity measurements below 1 K (Lasjaunias et al. 2003a). Moreover, we can use our heat capacity Cp data of the pristine samples as additional characterization information. The Cp behavior is very similar in both cases, the main difference lying in the contribution of catalyst particles detected below 1 K, of ferromagnetic Ni or Co, at a level of about 1 at.% or less. There is also a specific contribution to Cp as a power law in T, which cannot be ascribed to extrinsic impurities, but more probably to structural defects in the carbon lattice (graphene sheet), like pentagon/heptagon configurations. Its amplitude is smaller in the bucky-paper sample than in the AD-pallet sample.

For the adsorption measurements, samples are closed in a cell of dimensions adjusted to their shape, to minimize the dead volume. These sample cell volumes are $V_{\text{bucky-paper}} = 3$ cm^3 and $V_{\text{AD-pellet}} = 0.67$ cm^3. The procedure of out-gassing the samples is quite basic, i.e., to reproduce the conditions used for Cp measurements, that is after a heating around 50 °C under vacuum, one night of pumping with a turbo-molecular pump at ambient temperature to obtain a residual pressure of less than 10^{-6} mbar. To extract the adsorbed amount in SWNT, we performed P-V-T isotherms measurements at liquid nitrogen temperature with a home-built vacuum set-up, which consists of a calibrated volume separated from the sample cell by a valve. The admitted amount of gas (Kr or Ar) in the cell is determined by (i) measuring the pressure of this calibrated volume ($V = 17.5$ cm^3)

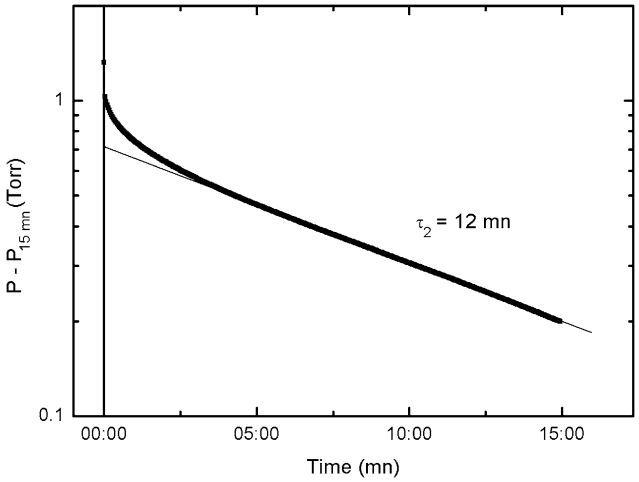

Fig. 2 Kr adsorption dynamics in the AD sample ($P_{15\,mn}$ is the measured pressure at 15 minutes). These data correspond to the absolute pressure pointed by the arrow in Fig. 3. The *straight line* shows the exponential decay with $\tau_2 = 12$ mn

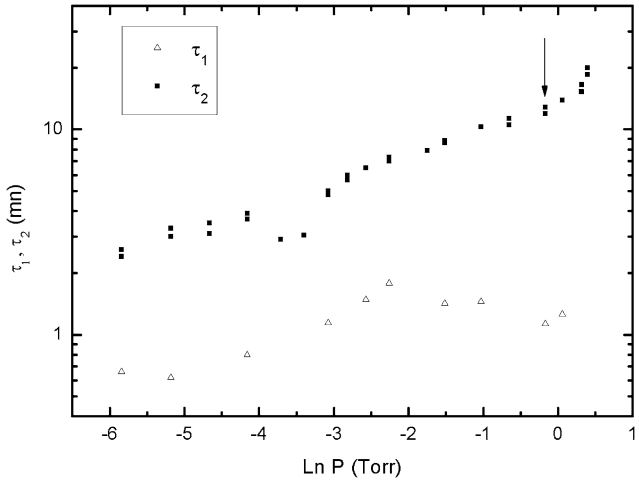

Fig. 3 The two time constants τ_1 and τ_2 of Kr adsorption as a function of pressure for the AD sample. The *arrow* shows the point of Fig. 2

with a Baratron-MKS capacitance manometer (up to 100 Torr with an accuracy around 10^{-4} Torr) the valve being closed, (ii) remeasuring the pressure when the valve to the sample cell is open, and (iii) correction of this pressure for thermomolecular effects.

We used a systematic procedure to achieve a very regular admission of gas versus time. Typically, we took data after waiting 10 minutes (or 15 minutes) in the low pressure range ($P < 0.04$ Torr), and 15 minutes (or 20 minutes for each sample, respectively) in the upper pressure range. Since we reached the equilibrium exponential decay regime (see Fig. 2), this time scales were long enough to obtain a systematic determination of the adsorbed gas amount. We presently note that the equilibrium time constant increases with increasing the accumulated adsorbed gas. In the case of Kr, this time constant was about 10 minutes for both NT samples at the maximum saturation pressure (see Fig. 3). These values are much larger than those of the empty cell (between 1 and 1.5 minutes) measured as reference in a separate experiment. We show in Fig. 3 the evolution of the two time constants τ_1 and τ_2 of the dynamics of Kr adsorption, as a function of the pressure, for the case of the AD-pellet. τ_1 and τ_2 correspond to the two successive exponential regimes, as shown by the plot of the pressure versus time (in Fig. 2). We suppose that the first regime corresponds to the admission of gas in the cell and its thermalisation, and the final regime (τ_2) to the mechanism of gas adsorption into the NT bundles.

3 Results

3.1 Argon adsorption

We present in Fig. 4 the Ar isotherms for the two samples measured at 77.3 ($\pm$0.1) K on a semi-logarithmic scale, for the pressure range from $2 \cdot 10^{-3}$ Torr to 90 Torr. We note that the maximum pressure is about two times lower than the saturated vapor pressure P_0 of Ar at 77 K ($P_0 = 188$ Torr), and hence does not influence the isotherm shape at high pressure.

From the first inspection of data, there occur two successive smooth steps for the bucky-paper sample (at $\ln P = -5$ and $\ln P \approx 1$), whereas for the AD-pellet a shallow bump centered at $\ln P \approx 0.5$ occurs; it seems there is not enough signal to distinguish the first step. The first step is ascribed to the highest binding energy sites, i.e. the quasi-linear channels as a few, large defective interstitial channels (IC's) (Bienfait et al. 2004; Shi and Johnson 2003) or the grooves between adjacent nanotubes on the external surface of the bundle. The second step is due to the completion of the first monolayer on the external surface. The ratio of the absorbate volume in the 1D channels and the surface is around 1/5 which is coherent with geometrical consideration (from the size of Ar and Kr atoms on the external surface between two next grooves). The midpoint of the steps which characterizes the binding energy of the two sites, can also be defined by the maximum of the derivative dN/dP, of the initial curve N(P) of the amount of adsorbate (here the STP volume V_{ads} in $cm^3 \cdot g^{-1}$ or $cm^3 \cdot g^{-1} \cdot$Torr) versus pressure. On the Fig. 5a for bucky-paper we clearly distinguish two inflexion points at $\ln P = -5$ and $\ln P = 0.7$, and on Fig. 5b for AD-pellet one local maximum at $\ln P = 0.5$.

These results are in excellent agreement with previous work using Ar as adsorbate (Talapatra and Migone 2001; Wilson et al. 2002). For Ar, interpolation of a series of adsorption isotherms of (Talapatra and Migone 2001) for $T = 77.3$ K yields completion of the first monolayer at $\ln P = 0.5$, and the isotherm at $T = 77.4$ K from (Wilson

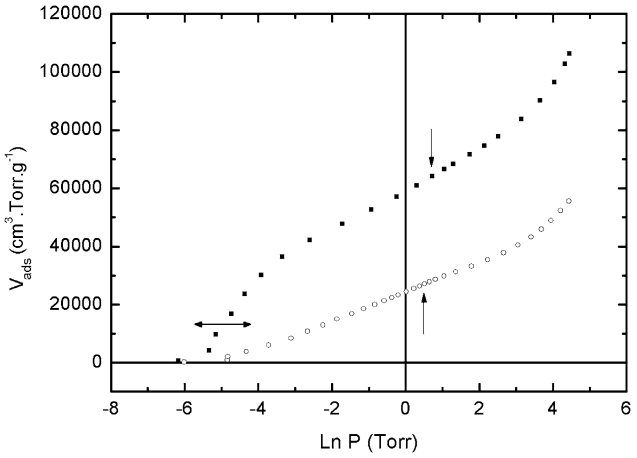

Fig. 4 Argon adsorption isotherms on the two samples (■ bucky paper, ○ AD-pellet) of CNT's at 77.3 K, per gram of sample. *Arrows* indicate the position of inflexion points determined by the derivation of data (Fig. 5). *Horizontal line* indicates the first step of adsorption for the bucky-paper sample

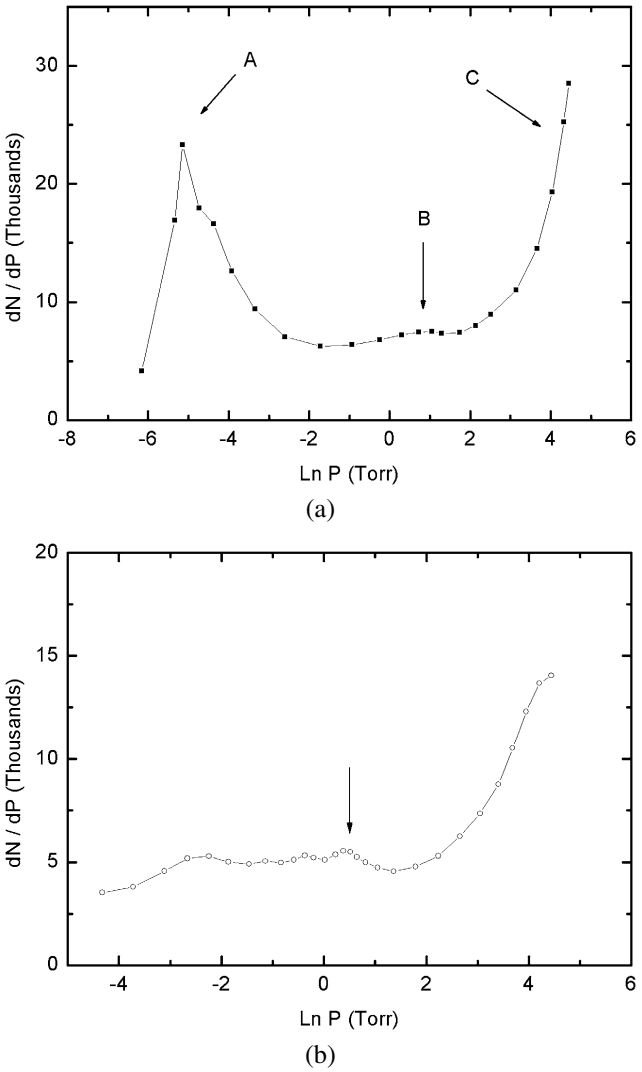

Fig. 5 Derivative of adsorbed Ar amount dN/dP from Fig. 4 as a function of pressure for the two samples. (**a**) For the bucky-paper sample, maximum (*A*) corresponds to the filling of the highest binding energy sites, like grooves or some interstitial channels. Local maximum (*B*) corresponds to the completion of the first monolayer, whereas the rising part (*C*) is the beginning of the second layer formation. (**b**) For AD-pellet, the local maximum at $\ln P = 0.5$ is ascribed to the first monolayer completion

et al. 2002) shows the inflexion point at $\ln P = 0.7$. We also obtain a rather good agreement with these references for the quasi-linear sites in the bucky-paper sample, either for the pressure of the first step or the relative amount of adsorbate in comparison to the monolayer completion (about 1/5). At this point, the overall agreement for the characteristics of the low energy sites for Ar adsorbate among at least 4 different samples of SWNT's (i.e. differently synthesized or from different batches) already shows the reproducibility of the binding energy of these sites and the quality of samples under investigation.

The second striking property directly evidenced from Fig. 4 is the large difference in the amount of adsorbate between the two samples. At the mid-steps of second site adsorption, the ratio is about 2.3 in favor to the bucky-paper sample. For our samples, the volume of adsorbate at the inflexion point is respectively 86 $cm^3 \cdot g^{-1}$ for bucky-paper, and 37 $cm^3 \cdot g^{-1}$ for AD-pellet. Using the same definition of adsorption capacity, we obtain 47 $cm^3 \cdot g^{-1}$ for the Ref. (Wilson et al. 2002) for a sample mass of 45 mg, and also 37 $cm^3 \cdot g^{-1}$ from Ref. (Talapatra and Migone 2001) for a sample mass of 290 mg (see Ref. Talapatra et al. 2002). Moreover, data from literature show a much larger spread of values for different synthesis techniques, for instance for HiPCO samples, as discussed later.

3.2 Krypton adsorption

We present in Fig. 6(a, b) the Kr isotherms for the two samples at the temperature of 77.2 K for the bucky-paper and 77.3 K for the AD-pellet, on a semi-logarithmic scale in the range of pressure between 10^{-4} Torr and the saturated vapor pressure of Kr:$P_0 = 1.74$ Torr ($\ln P_0 = 0.554$) at 77.2 K, which is clearly seen for the bucky-paper sample. Due to the much lower P_0 for Kr in comparison to Ar, we are unable to detect the first step (IC and groove sites) in the isotherm which is shifted to lower pressure, estimated around $5 \cdot 10^{-5}$ Torr ($\ln P = -10$) from (Gatica et al. 2001; Muris et al. 2000). Indeed such a low pressure is smaller than the accuracy of the MKS-Baratron (10^{-4} Torr), which results in an uncertainty increasing rapidly for $\ln P \leq -7$. For instance, below $\ln P = -8$, the uncertainty become larger than one decade. These very low pressure measurements are only indicative. However, the cumulated adsorbed volumes are so small that the influence on the analysis of isotherms at higher pressure is negligible. In the bucky-paper sam-

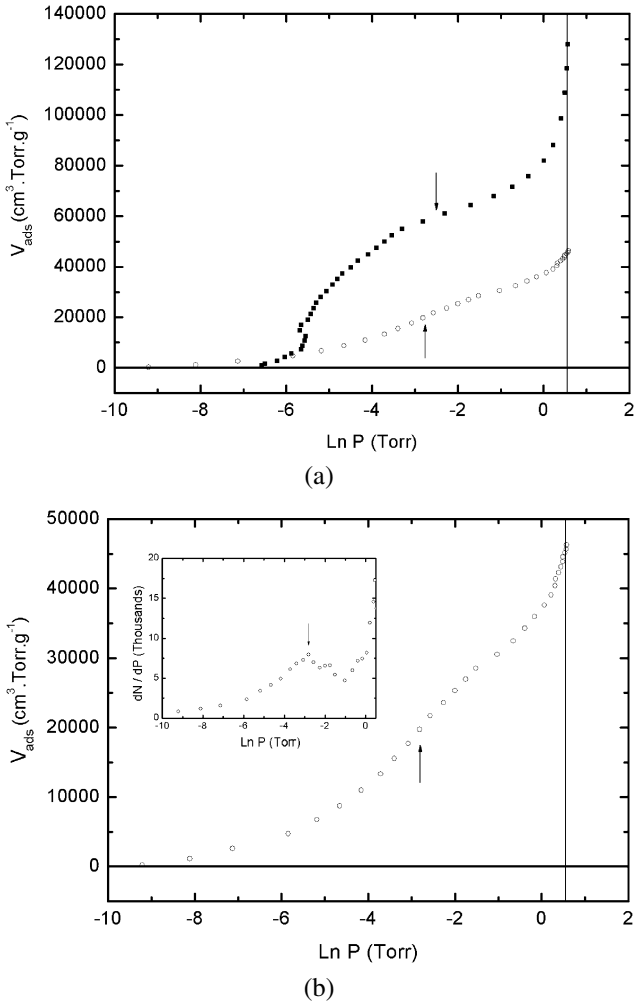

Fig. 6 (**a**) Krypton adsorption isotherms on the two samples for bucky paper (■) at 77.2 K and for AD-pellet (○) at 77.3 K. *Arrows* indicate the adsorbed volume at the completion of the first monolayer. In (**b**) for AD-pellet, the inflexion point is determined by the derivation of data (see the *inset*). The *vertical lines* represent the Kr saturated vapor pressure P_0

ple, the mid-step which corresponds to the first monolayer completion is well observed with an inflexion point around $\ln P = -2.5$ (Fig. 6a). For the AD-pellet, this step is not so obvious from the raw data. The inflexion point obtained from the derivative dN/dP yields $\ln P = -2.8$ close to the value for bucky-paper. Like in the Ar case, the adsorption capacity is much larger for the bucky-paper sample. Above the inflexion point, i.e. in the P-range used for the "BET-like" analysis (see Sect. 3.3), the ratio of adsorbed amount varies from 2.5 to 2.2 (up to $P = 1.25$ Torr). Estimation of the volume of adsorbate around the inflexion point, i.e. at monolayer completion, yields 79–80 $cm^3 \cdot g^{-1}$ for bucky-paper, and 26 to 33 $cm^3 \cdot g^{-1}$ for AD-pellet, taking in account the uncertainty of the determination. Again, there is a large difference in the adsorption capacity between the two samples for Kr.

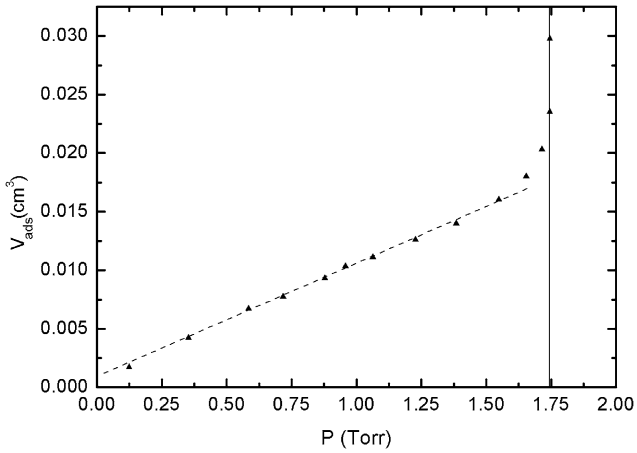

Fig. 7 Kr adsorbed volume in the empty cell used for the bucky paper sample

One can wonder whether the second rapid increase of V_{ads}, especially for the bucky-paper sample, above $P = 1$ Torr is not only due to the proximity of the limiting pressure P_0. In order to test our experimental conditions, including the dynamics of adsorption, we have measured the empty cell used for the bucky-paper sample (see Fig. 7, in linear scale): there is a linear increase of V_{ads} versus pressure up to 1.55 Torr, above it V_{ads} increases more rapidly to reach $P_0 = 1.745$ Torr. So, the second rapid increase of V_{ads} which starts already at 1 Torr in the bucky-paper indicates a new site filling, which can only be the beginning of the second layer.

Our previous conclusion about the similarity of the sites binding energies of the two kinds of samples are corroborated by the Kr study.

3.3 Analysis by the "BET" method: estimation of specific surface areas

Another systematic method to evaluate the amount of adsorbed gas, and hence the specific surface area of different adsorbates, is the usual BET method (Robertson et al. 1983; Yano et al. 1998). This method consists of fitting the experimental data in the form: $y = x/[V_{ads}(1 - x)]$ versus $x = P/P_0$, by a linear variation, valid for x between 0.05 and 0.3. We show in Fig. 8 such a fit of data of Kr adsorbed in the AD-pellet. The linear law is well obeyed for $0.01 < x < 0.15$, which yields an adsorbed amount for the monolayer completion of 35.5 $cm^3 \cdot g^{-1}$. A similar quality of fitting is obtained in the same P-range for Kr in bucky-paper sample which yields to 78 $cm^3 \cdot g^{-1}$. Both values are in agreement with our previous estimation from the direct diagram V_{ads} versus $\ln P$. However, in the case of Ar the linear fits in the range $0.025 < x < 0.20$ yield values which can be 20% larger than the previous determination.

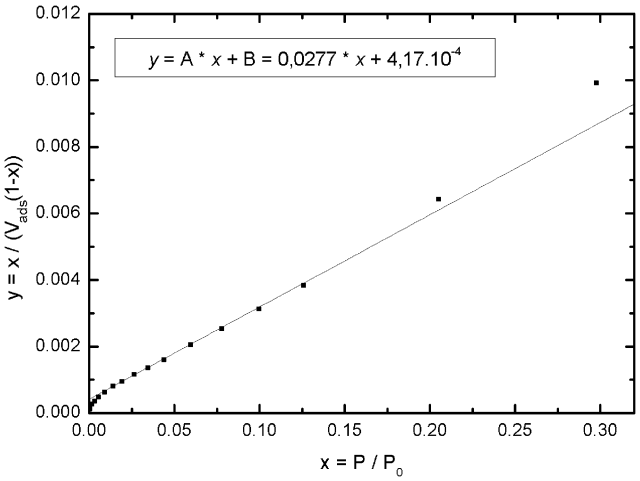

Fig. 8 BET plot for Kr isotherm on the AD-pellet sample

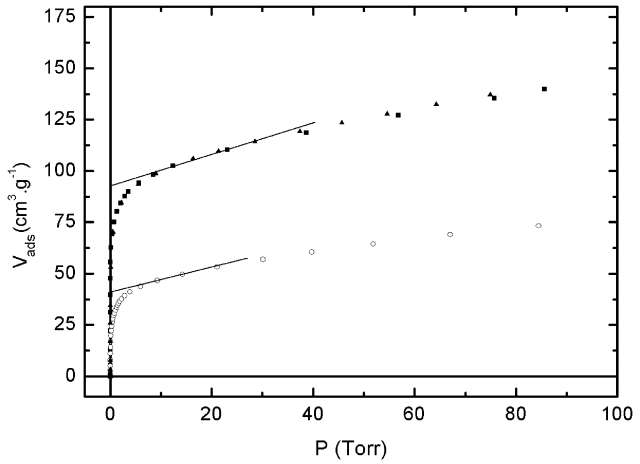

Fig. 9 Argon adsorption isotherms (■, ▲: 2 experiments on Bucky paper, ○ AD-pellet) at 77.3 K. "Point A" is defined at the intersection of the straight line and the zero pressure axis

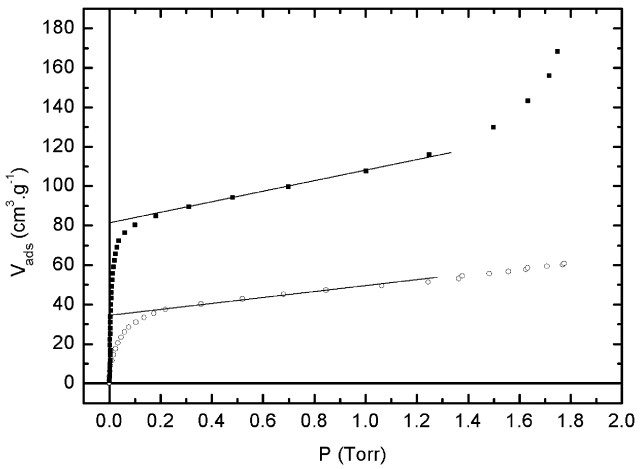

Fig. 10 Krypton adsorption isotherms (■ bucky paper at 77.2 K, ○ AD-pellet at 77.3 K)

We therefore used a more direct method, based on the linear diagram $V_{ads}(P)$ (Figs. 9 and 10). There are two possible ways of estimating the monolayer completion, also using data for $P/P_0 < 0.3$: a linear regime obeyed in the low-P range can be extrapolated to the zero pressure axis which yields the value V_A (called "point A" method); the second one is to estimate the lower limit of the linear regime: this gives V_B (called "point B" method). As seen in Figs. 9 and 10, there is only a little difference between V_A and V_B, by around 10%. Taking in account the rather short P interval where there is a linear regime in the case of Ar, the error is lower in the estimation of V_A. In the case of Kr, the condition $P/P_0 < 0.3$ would limit the analysis to $P < 0.6$ Torr, but we see that linearity is obeyed up to much larger values.

Values of V_A are reported in Table 1, and compared to the previous analysis by the BET method and inflexion point: the agreement is generally good. In order to estimate the amount of the monolayer completion, the group of S. Talapatra et al. (Krungleviciute et al. 2004) used the "point B" determination. When we compare the case of Ar to ours, the difference between A and B determination is also less than 10%. At this step, we outline that we find the same ratio for the adsorption capacity in both samples, either for Ar or Kr adsorbate.

From the monolayer completion values, we can extract the specific surface areas. For that, we have to use estimates of the area σ occupied by one atom of the adsorbate on the outer graphene surface of the CNT. In order to compare to the other determination performed on CNT's (Krungleviciute et al. 2004), we use the similar assumption that σ is the same as measured on planar graphite. We use $\sigma = 13.2$ Å^2 for Ar (Taub et al. 1975; McTague et al. 1982), and 15.2 Å^2 for Kr (McTague et al. 1982; Rouquerol et al. 1999). Specific surface areas in $m^2 \cdot g^{-1}$ are reported on Table 1 with values of around 140 $m^2 \cdot g^{-1}$ for AD-pellet and 325 $m^2 \cdot g^{-1}$ for bucky-paper.

4 Discussion

The first conclusion is that the specific areas are similar for Ar and Kr adsorbates on a same kind of sample, as for the binding energy on the external surface for monolayer completion. The group of Talapatra et al. previously reached the same conclusion for Ne, Ar, Xe and CH_4 adsorbed on HiPCO-CNT samples (Krungleviciute et al. 2004). Due to the large variations in the atomic size of these adsorbates, they concluded that only the grooves and outer surface sites were available in these samples. Hence, only a few, larger size, defective interstitials are possible additional sites for heterogeneous bundles. The case of much smaller size atoms, like He, is interesting to compare and we discuss this point later.

Table 1 Amount of adsorbate (Ar and Kr) at first monolayer completion expressed in $cm^3 \cdot g^{-1}$ and in $mmol \cdot g^{-1}$ (to compare to other literature data), and estimated specific surface area for the two samples (for the calculation, we use 1 $cm^3 \cdot Torr = 3.54 \cdot 10^{16}$ atoms)

Adsorbate species	Sample	Amount of adsorbate				Area/molecule on graphite	Specific surface area ($m^2 \cdot g^{-1}$) (from "point A")
		(a) estimated at mid-point step in $cm^3 \cdot g^{-1}$	(b) BET method in $cm^3 \cdot g^{-1}$	(c) "point A" method			
				in cm^3/g	in mmol/g		
Ar	Bucky-paper (Rice)	86	95	91.5 ±0.5	4.09 ±0.02	13.2 Å^2	325 ±2
	AD-Pellet (Montpellier)	37	50	40.5 ±0.5	1.79 ±0.02		144 ±2
Kr	Bucky-paper (Rice)	79.5 ±0.5	78	80.5 ±0.5	3.60 ±0.02	15.2 Å^2	329 ±2
	AD-Pellet (Montpellier)	29.5 ±3.5	35.5	34.5 ±0.5	1.54 ±0.02		141 ±2

A second point to outline is the large difference in the specific surface areas between the two kinds of samples, and again, this difference does not depend on the adsorbate species: here by a factor 2.3, in favor of the bucky-paper sample. This property confirms our previous conclusions from our calorimetric studies performed on the same kinds of samples with ^{4}He as adsorbate (Lasjaunias et al. 2002, 2003a, 2003b).

It is difficult to reconcile this difference with the topology of bundles, i.e. their larger size for the bucky-paper in comparison to the AD-pellet, if one supposes that in both cases nanotubes are closed-ended. Obviously the ratio of the external surface adsorption, including the grooves, per unit mass decreases when the bundle size increases. However, whereas the Montpellier samples being not purified, one has the assurance that they are closed-ended, for the bucky-paper "Rice" ones, the purification by acid can induce that a portion of the tubes are open-ended (which therefore offers the possibility of new adsorption sites), estimated at maximum of 20–30%. We can compare our total adsorption capacity to MER SWNTs (Rols et al. 2005), where almost *all* tubes are open-ended, also with Ar adsorbate. For the first step (i.e. highest binding energy sites), which involves the inner tubes sites in addition to IC's and grooves, they measured an adsorption capacity of 5 $mmol \cdot g^{-1}$ much larger than in our sample with a *total* adsorption of 4.1 $mmol \cdot g^{-1}$ (Table 1). This leads us to the conclusion that we have probably less than 20% of open-ended tubes in our bucky-paper sample. A possible role of the impurities at the origin of the difference of adsorption capacity is to be ruled out, since all characterization and specific heat experiments indicate less impurities present in the bucky-paper sample, at the exception of residual Co particles, which could not intervene in the adsorption processes.

A rather surprising property of the MER samples is that the binding energies for Ar are very close to those measured in closed-ended bundles (Bienfait et al. 2003), despite a greater variety of possible adsorption sites, including now those located *inside* the tubes. Indeed, one observes only two values of isosteric heat (i.e. of binding energy) in the open-ended tubes, like in the closed-ended, but with a difference in the extent of the first plateau (highest binding energy: See Ref. Rols et al. 2005) for the open-ended ones corresponding to a larger adsorption capacity. The authors conclude to similar adsorption energies for most of the internal sites than the external grooves or ICs, all being linear-like chains of Ar atoms. More evidently, the binding energies on the outer graphene surfaces are similar. Our results are in agreement with this conclusion, proving the similarity of binding energies—either for Ar or Kr—in the two kinds of samples.

There exists a wide spread of the effective surface values in the literature. We have indicated the good agreement for Ar adsorbate between several samples, all synthesized by the arc-discharge Montpellier technique (Journet et al. 1997; Rols et al. 1999). A small effective area of 38 $m^2 \cdot g^{-1}$ for Ne and 41 $m^2 \cdot g^{-1}$ for Xe was also reported in samples of this origin by the group of Talapatra (Talapatra et al. 2000), whereas a much larger value of 204 $m^2 \cdot g^{-1}$ was reported by M. Muris et al. (Muris et al. 2000) for CH_4. Finally the HiPCO nanotubes show, to our knowledge, the largest values (determined by reference to graphite) of 450 to 468 $m^2 \cdot g^{-1}$, for different adsorbates including Ar (Krungleviciute et al. 2004). It is probable that in this latter case, a fraction of the nanotubes is open-ended. To our knowledge, there are no other published data of adsorption isotherms on the "Rice" bucky-paper.

We now discuss the case of ^{4}He adsorbate, that we have previously investigated by calorimetric measurements in the low-T range (100 mK–6 K). We also observed a large dif-

ference in the adsorption capacity between the two kinds of samples. The maximum adsorption amount (corresponding to $7 \cdot 10^{19}$ atoms adsorbed) was 1.3 mmol·g^{-1} for the AD-pellet compared to 2.6 mmol·g^{-1} for bucky-paper. These values are lower than those determined from the adsorption isotherms of Ar and Kr. Despite that these concentrations are less precise than those given by the present isotherm technique, we recover the factor of two between the two kinds of samples. There is also a larger amplitude for the low-T heat capacity of the adsorbate in the maximum adsorption regime (see Fig. 2 in Lasjaunias et al. 2003a), which is characterized by a quasi-linear variation in T for both samples. When the heat capacity is defined per atom of adsorbate, there remains a factor of about two in favor of the bucky-paper sample. There is no direct correlation between these calorimetric results and the effective surface area of the samples, in particular it is possible for ^{4}He to fill the interstitial channels, which can contribute substantially to the heat capacity (Lasjaunias et al. 2003b), but this supports our present conclusion of a larger contribution or adsorption capacity in the bucky-paper species.

An interesting property, which has not yet been pointed out, is the *striking similarity* of the neutron diffraction spectra of the Ar and ^{4}He adsorbates on different kinds of SWNTs (Pearce et al. 2005; Rols et al. 2005; Bienfait et al. 2003), indifferently close or open-ended. In the range of wave-vectors investigated ($1.5\ \text{A}^{-1} < Q < 5\ \text{A}^{-1}$), two broad peaks occur which are centered at *exactly* the same Q values, and with a very similar broadening which hints for a similar structural disorder for the two adsorbates (Ar and ^{4}He). These two peaks are the best defined at the first monolayer completion. In one sample (Bienfait et al. 2003) prepared by AD in Montpellier, similarly as ours, and hence with closed-ended tubes, the corresponding coverage for Ar is 2.7 mmol·g^{-1} which compares well to our coverage value. Another kind of sample was used for the study of ^{4}He adsorption by neutron diffraction at $T = 2.5$ K (Pearce et al. 2005): it was "Bucky-Pearls TM", supposed with the same manufacture process as for HiPCO bundles, and hence with probably a fraction of open-ended tubes. In that case, the monolayer completion on the bundles surface is complete for ≈220 cm^3·g^{-1}(or 9.8 mmol·g^{-1}), again a very large value in comparison to the closed-ended AD samples, and more than two times larger than our "Rice" bucky-paper. Finally, an open-ended MER sample was also studied by neutron diffraction with Ar as adsorbate, with a maximum coverage of about 9 mmol·g^{-1} (Rols et al. 2005). In all three cases, raw neutron diffraction data of the adsorbate are very similar, despite the wide range of the coverage values. These spectra were analyzed by combination of 1D (linear chains) and 2D sites. The arrangement of the adsorbate appear to be very similar either in close or open-ended tubes, and doesn't depend on the nature of the adsorbate. The broadening of the diffraction peaks is ascribed either to inhomogeneities of the substrate, for instance a distribution of tubes diameters (Pearce et al. 2005), or to the disorder in the arrangement of adsorbate atoms themselves (Rols et al. 2005).

5 Conclusions

From our adsorption isotherm experiments of Ar and Kr in two different kinds of SWNT bundles, we can conclude that the adsorption process, i.e. the progressive filling of the available sites and the binding potential of these sites, is very similar for the two gas species. The effective adsorption surface areas differ by a factor of more than two between the two kinds of samples. The higher adsorption capacity of the bucky-paper sample, probably due to a fraction of open-ended tubes, confirms our previous findings from low-T heat capacity measurements in the case of ^{4}He adsorbate on the same kinds of sample. However, from this comparison we cannot assert that the adsorption sites are similar for ^{4}He as for Ar and Kr. The broad range of adsorption capacity by a factor of ten among SWNT samples prepared by different ways (purified or not), remains to be clarified in connection with the bundle topology, or with the presence of open-ended tubes.

Acknowledgements We want to acknowledge H. Godfrin and J. Bossy for helpful discussions and experimental advices, J.L. Sauvajol and J.E. Fischer for supplying samples and informations about the synthesis.

References

Almairac, R., Sauvajol, J.L.: University of Montpellier, private communication (2002)

Bienfait, M., Zeppenfeld, P., Dupont-Pavlovsky, N., Palmari, J.P., Johnson, M.R., Wilson, T., DePies, M., Vilches, O.E.: Adsorption of argon on carbon nanotube bundles and its influence on the bundle lattice parameter. Phys. Rev. Lett. **91**, 035503–035507 (2003)

Bienfait, M., Zeppenfeld, P., Dupont-Pavlovsky, N., Muris, M., Johnson, M.R., Wilson, T., DePies, M., Vilches, O.E.: Thermodynamics and structure of hydrogen, methane, argon, oxygen, and carbon dioxide adsorbed on single-wall carbon nanotube bundles. Phys. Rev. B **70**, 035410–035420 (2004), and references therein

Gatica, S.M., Bojan, M.J., Stan, G., Cole, M.W.: Quasi-one- and two-dimensional transitions of gases adsorbed on nanotube bundles. J. Chem. Phys. **114**, 3765–3769 (2001)

Journet, C., Maser, W.K., Bernier, P., Loiseau, A., Lamy de la Chapelle, M., Lefrant, S., Deniard, P., Lee, R., Fisher, J.E.: Large scale production of single-walled carbon nanotubes by the electric-arc technique. Nature (London) **388**, 756–758 (1997)

Krungleviciute, V., Heroux, L., Talapatra, S., Migone, A.: Gas adsorption on HiPco nanotubes: surface area determinations, and neon second layer data. Nanoletters **4**, 1133–1137 (2004)

Lasjaunias, J.C., Biljakovic, K., Benes, Z., Fisher, J.E., Monceau, P.: Low-temperature specific heat of single-wall carbon nanotubes. Phys. Rev. B **65**, 113409–113413 (2002)

Lasjaunias, J.C., Biljakovic, K., Monceau, P., Sauvajol, J.L.: Low-energy vibrational excitations in carbon nanotubes studied by heat capacity. Nanotechnology **14**, 998–1003 (2003a)

Lasjaunias, J.C., Biljakovic, K., Sauvajol, J.L., Monceau, P.: Evidence of 1D behavior of He^4 confined within carbon-nanotube bundles. Phys. Rev. Lett. **91**, 025901–025905 (2003b)

McTague, J.P., Als-Nielsen, J., Bohr, J., Nielsen, M.: Synchrotron x-ray study of melting in submonolayer Ar and other rare-gas films on graphite. Phys. Rev. B **25**, 7765–7772 (1982)

Muris, M., Dufau, N., Bienfait, M., Dupont, N., Grillet, Y., Palmari, J.P.: Methane and krypton adsorption on single-walled carbon nanotubes. Langmuir **16**, 7019–7022 (2000)

Pearce, J.V., Adams, M.A., Vilches, O.E., Johnson, M.R., Glyde, H.R.: One-dimensional and two-dimensional quantum systems on carbon nanotube bundles. Phys. Rev. Lett. **95**, 185302–185306 (2005)

Robertson, R.J., Guillon, F., Harrison, J.P.: Properties of sintered submicron copper and silver powders and their relation to low temperature heat exchangers. Can. J. Phys. **61**, 164–176 (1983)

Rols, S., Almairac, R., Henrard, L., Anglaret, E., Sauvajol, J.L.: Diffraction by finite-size crystalline bundles of single wall nanotubes. Eur. Phys. J. B **10**, 263–270 (1999)

Rols, S., Benes, Z., Anglaret, E., Sauvajol, J.L., Papanek, P., Fisher, J.E., Coddens, G., Schober, H., Dianoux, A.J.: Phonon density of states of single-wall carbon nanotubes. Phys. Rev. Lett. **85**, 5222–5225 (2000)

Rols, S., Johnson, M.R., Zeppenfeld, P., Bienfait, M., Vilches, O.E., Schneble, J.: Argon adsorption in open-ended single-wall carbon nanotubes. Phys. Rev. B **71**, 155411–155419 (2005)

Rouquerol, F., Rouquerol, J., Sing, K. (eds.): Adsorption by Powders and Porous Solids: Principles, Methodology and Applications, p. 171. Academic (1999)

Shi, W., Johnson, J.K.: Gas adsorption on heterogeneous single-walled carbon nanotube bundles. Phys. Rev. Lett. **91**, 015504–015508 (2003)

Stan, G., Bojan, M.J., Curtarolo, S., Gatica, S.M., Cole, M.W.: Uptake of gases in bundles of carbon nanotubes. Phys. Rev. B **62**, 2173–2180 (2000)

Talapatra, S., Krungleviciute, V., Migone, A.D.: Higher coverage gas adsorption on the surface of carbon nanotubes: evidence for a possible new phase in the second layer. Phys. Rev. Lett. **89**, 246106–246110 (2002)

Talapatra, S., Migone, A.D.: Existence of novel quasi-one-dimensional phases of atoms adsorbed on the exterior surface of closed-ended single wall nanotube bundles. Phys. Rev. Lett. **87**, 206106–206110 (2001)

Talapatra, S., Zambano, A.Z., Weber, S.E., Migone, A.D.: Gases do not adsorb on the interstitial channels of closed-ended single-walled carbon nanotube bundles. Phys. Rev. Lett. **85**, 138–141 (2000)

Taub, H., Passell, L., Krems, J.K., Carneiro, K., McTague, J.P., Dash, J.G.: Neutron-scattering studies of the structure and dynamics of ^{36}Ar monolayer films adsorbed on basal-plane-oriented graphite. Phys. Rev. Lett. **34**, 654–657 (1975)

Wilson, T., Tyburski, A., De Pies, M.R., Vilches, O.E., Becquet, D., Bienfait, M.: Adsorption of H_2 and D_2 on carbon nanotube bundles. J. Low Temp. Phys. **126**, 403–408 (2002)

Yano, H., Yoshizaki, S., Ingaki, S., Fukushima, Y., Wada, N.: Observation of superfluid ^4He adsorbed in one-dimensional mesopores. J. Low Temp. Phys. **110**, 573–578 (1998)